Waveform-Dependent Absorbing Metasurfaces

Hiroki Wakatsuchi,* Sanghoon Kim, Jeremiah J. Rushton, and Daniel F. Sievenpiper†

Applied Electromagnetics Group, Electrical and Computer Engineering Department, University of California, San Diego, California 92093, USA

(Received 9 September 2013; published 10 December 2013)

We present the first use of a waveform-dependent absorbing metasurface for high-power pulsed surface currents. The new type of nonlinear metasurface, composed of circuit elements including diodes, is capable of storing high-power pulse energy to dissipate it between pulses, while allowing propagation of small signals. Interestingly, the absorbing performance varies for high-power pulses but not for high-power continuous waves (CW's), since the capacitors used are fully charged up. Thus, the waveform dependence enables us to distinguish various signal types (i.e., CW or pulse) even at the same frequency, which potentially creates new kinds of microwave technologies and applications.

DOI: 10.1103/PhysRevLett.111.245501 PACS numbers: 81.05.Xj

Conventional absorbers [1,2] are independent of incoming power levels and therefore absorb not only destructive high-power signals but also small signals necessary for antenna communications. These two effects can be decoupled by introducing nonlinearity into a periodic structure or metasurface [3] such that the artificially engineered surface possesses a low-power surface impedance that is different from its high-power absorbing response. Furthermore, we can take advantage of the fact that high-power microwave signals generally come from pulsed sources and design a structure in which the high-power microwave energy is rectified and stored as a static field in the surface and then dissipated between pulses. This provides freedom in the choice of lossy components, allowing us to further decouple the high-power absorption properties from the small-signal behavior and also design the surface to respond specifically to short pulses.

Many nonlinear metamaterials and metasurfaces derive their nonlinear properties from altering the resonant paths of induced electric currents with nonlinear media (e.g., through semiconductive substrates [4–7] or geometrical modifications induced by heating [8] or magnetic force [9,10]). These differ from our nonlinear metasurfaces based on diodes or *nonlinear circuits*. Diodes switch between nonconducting and conducting states depending on the applied voltage and therefore are capable of handling incoming signals differently depending on the magnitude. Because diodes rectify high-power signals and convert much of the energy to a static field, our nonlinear metasurfaces perform differently from others that convert incoming signals into high-order modes [11,12] or exploit wave-mixing techniques [13].

To understand how such a structure absorbs high-power pulse energy, consider Figs. 1(a) and 1(b). Our metasurface is composed of circuit components (i.e., diodes, capacitors, and resistors) as well as a conductive ground plane and periodic metal patches, separated by a dielectric substrate (Rogers 3003). During a pulse [i.e., Fig. 1(a)] high-power surface currents propagate on the patches. Once the voltage difference across a diode reaches the turn-on voltage, electric charges flow into a capacitor and the energy is stored. Between pulses [Fig. 1(b)] the stored electric charges are dissipated in a resistor. Note that the metasurface does not respond to small signals and therefore behaves as an ordinary metal surface, since the voltage difference is not large enough to turn on the diodes. Although we have demonstrated absorbing behavior based on rectification previously [14,15], the new metasurface demonstrated here has three important differences. First, the previous metasurfaces contained vertical conducting vias and, thus, were not planar. In contrast, the structures designed here contain no vias and are entirely printed on the top surface of the substrate. This may facilitate integration with other structures such as composite vehicle or aircraft skins. Second, the new surface provides full-wave rectification using a four-diode bridge circuit, increasing the efficiency of microwave conversion into the static field (see Supplemental Material [16]). Third, the new configuration has the parallel *RC* circuit entirely isolated from the resonant structure by diodes. As a result, the self-resonance frequency of the capacitors does not affect the low-power response of the surface. Without this feature, we would be unable to use sufficiently large capacitors to fully store the pulse energy without introducing unwanted behavior into the low-power absorption or scattering response.

The metasurface in Figs. 1(a) and 1(b) was realized using the printed structure shown in Fig. 1(c). The structure was built on a 1.52 mm thick Rogers 3003 substrate. The periodicity of the printed metal pattern was 18 mm. A 10 kΩ resistor and 1 nF capacitor were attached at the gap between two small patches which were separated from the larger main patches by pairs of diodes forming a full-wave rectification circuit. Note that the resistance value was set large enough to prevent significant direct dissipation from the diodes, although the suitable resistance value depends on several factors including the metasurface

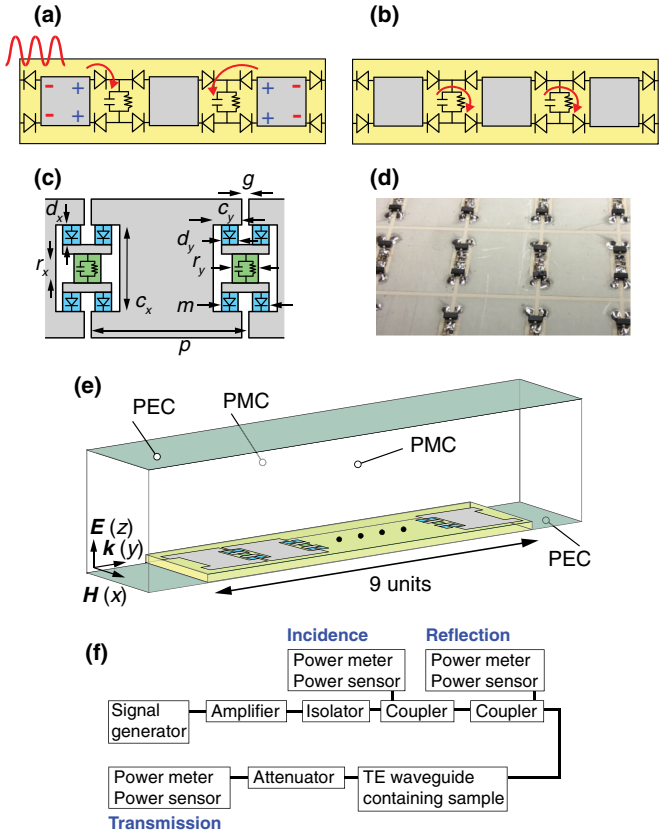

FIG. 1 (color online). Circuit-based nonlinear metasurface absorber. Response (a) during a pulse and (b) between pulses. The metasurface stores the energy of the high-power pulse in capacitors during the illumination, while between pulses discharging the energy into resistors. (c) The geometry simulated. The periodic units were build on a 1.52-mm-high dielectric substrate (Rogers 3003), which had a conductive ground plane on another side. The dimensions were given from $c_x = 7.6$, $c_y = 1.7$, $d_x = 1.3$, $d_y = 0.5$, $g = 1.0$, $m = 2.4$, $p = 18.0$, $r_x = 1.0$, and $r_y = 2.0$ mm. (d) Measurement sample. All the circuit components were soldered to the periodically metalized surface. (e) TEM waveguide simulation. The metasurface illustrated in (c) is placed at the bottom of the waveguide (22 mm tall and 18 mm wide). (f) Measurement system for pulse measurement. The number of periodic units deployed along the incident magnetic field was varied depending on the width of the TE waveguides used (WR284 or WR187) so that the structure fully occupied the bottom surface between the sidewalls. See Supplemental Material [16] for more details on (e) and (f).

design and operating frequency. Capacitors were modeled to have a self-resonant frequency at 0.3 GHz. Use of larger capacitance enables us to store more energy. However, this delays the discharge process of the capacitors due to increase of the time constant. The operating frequency of the metasurface is scalable by changing the periodicity, as long as the switching speed of the diodes used is fast enough to respond to the incoming signal. More details on the structural configuration are summarized in Fig. 1(c). Numerical simulations were performed by electromagnetic-circuit cosimulation in the same manner as our early work (see Ref. [14] and Supplemental Material [16]). In this simulation we placed nine units of the periodic structure (i.e., 162 mm long in total) on the bottom of a transverse electromagnetic (TEM) waveguide (22 mm tall and 18 mm wide).

The measurement sample is shown in Fig. 1(d). The sample was fabricated to have the same conditions as the simulation model except for a few points. For example, the measurement needed to be performed with a finite width of transverse electric (TE) waveguide (WR284 or WR187). Hence, the measurement samples were designed to have a multiple number of periodic units for the direction of the incident magnetic field as well to fully occupy the bottom of the waveguides. Additionally, the measurement sample included Schottky diodes (Avago; high frequency detector diodes HSMS-2863/2864), which were included as a SPICE model in the simulation. The measurement was performed with two systems, respectively, for low-power and high-power measurements including high-power pulses. For the low-power measurement a network analyzer (Agilent E5071C) was connected to the two ends of a TE rectangular waveguide containing the sample. The measurement system used for the high-power measurement is depicted in Fig. 1(f). The details are described in Supplemental Material [16].

Simulation results of the low-power scattering and absorption profile are shown in Fig. 2(a). As seen in this figure, the metasurface mostly transmitted the low-power signal with some limited absorption around 4.4 GHz. However, once the input signal was switched to 50 ns high-power pulses, an absorptance peak emerged more strongly as plotted in Fig. 2(c). For instance, around 4.4 GHz the absorptance reached almost 100% with 10 to 15 dBm pulses. Further increasing the input power reduced the absorptance a little but resulted in relatively broadband behavior. Also note that at 4.2 GHz, where the low-power transmittance was more than 80%, the absorptance was increased from below 20% to more than 80%. The behavior of the nonlinear metasurface changed from a relatively low-loss surface to an absorptive surface due to the combination of rectification and the energy storage in the capacitors. A proof of the rectification to a static field is seen in Supplemental Material [16]. Another point is that the absorption is reduced for CW signals as seen in Fig. 2(e). This is because rectification ceases once the capacitors are charged up to the level of the incoming signal. The high-power CW performance is controllable by varying the resistance values (see Supplemental Material [16]); i.e., more dissipation occurs by reducing the resistance value, which permits direct energy dissipation during rectification. In Fig. 2(e), however, we maximized the pulse effect, i.e., the contrast between high-power pulse and high-power CW, which is a distinctive feature of our nonlinear metasurface compared to other nonlinear metasurfaces (e.g., [4–6]).

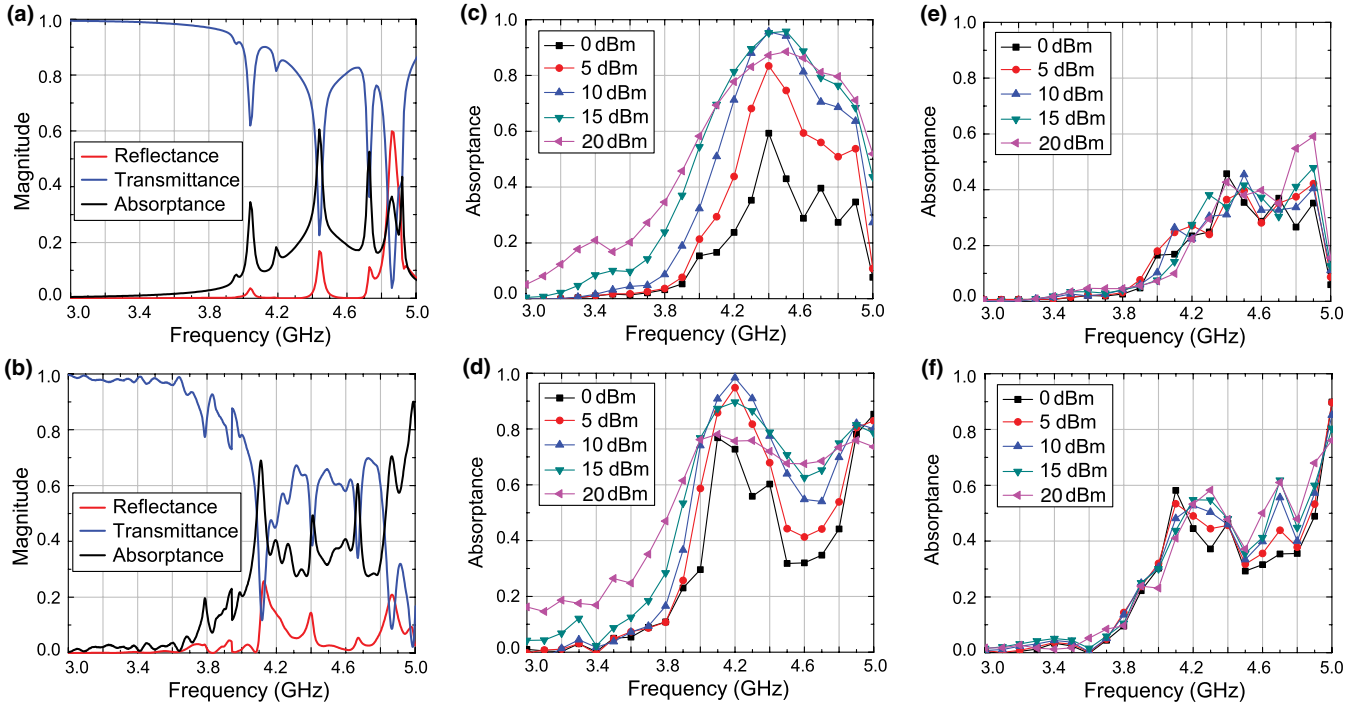

FIG. 2 (color online). Scattering and absorbing profile. Simulation results are plotted in the top figures [i.e. (a),(c), and (e)], while measurement results in the bottom [(b), (d), and (f)]. Low-power CW responses are shown in (a) and (b). High-power pulse absorptances are shown in (c) and (d), while high-power CW absorptances in (e) and (f). In (c) and (d) the pulse width was set to 50 ns.

The numerical results were then validated by measurement results. Figure 2(b) shows almost the same characteristics as Fig. 2(a) but with a minor low-frequency shift and slightly reduced transmittance around 4.4 GHz. These discrepancies can be mainly attributed to parasitic circuit parameters (especially in the diodes), which were not modeled in the simulation. However, the absorbing performance was still significantly enhanced as in the simulation, once the input source was switched to high-power pulses [Fig. 2(d)]. A strong absorptance peak was observed at 4.2 GHz with a 10 dBm pulse, while further increase of the input power resulted in a small reduction but with broadband behavior. Also, at 4.0 GHz the metasurface absorbed 80% of the 15 dBm pulse energy, while transmitting the same percentage of a low-power signal. Thus, the measurements validate the simulations and demonstrate that the surface is transformed from relatively low loss to highly absorbing under high-power illumination. Also note that the absorbing performance was reduced when the input signal was changed from high-power pulses to high-power CW signals [Fig. 2(f)] as expected. The relatively large absorptance seen around 5.0 GHz is assumed to be due to parasitics of the diode packages. Therefore, the absorptance value remained the same with various input powers.

The transition between a 50 ns pulse and CW was more clearly investigated in Fig. 3(a). In this simulation the pulse width was varied from 50 ns to 10 μs. As seen in this figure the absorptance curve nearly saturated at 10 μs, which agrees with the time constant τ derived from the capacitance C and resistance R used, i.e., $\tau = RC = 10\ \mathrm{k\Omega} \cdot 1\ \mathrm{ns} = 10\ \mu\mathrm{s}$. Also, the saturated absorptance at 10 μs (i.e., 0.31) was close to the high power CW performance (i.e., 0.28) [see Fig. 2(e)]. Similar trends were observed in the measurement [see Fig. 3(b)]. A minor delay of the saturation can be explained by some parasitic parameters in the circuit components, which increased the time constant slightly. However, the 10 μs absorptance (i.e., 0.32) was still in proximity with the CW result (i.e., 0.30) [see Fig. 2(f)]. For these waveform dependences,

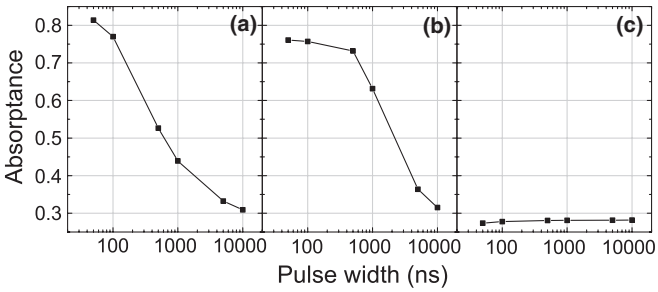

FIG. 3. Absorptance dependence on pulse width. (a) Simulation result at 4.2 GHz and (b) measurement result at 4.0 GHz with a 15 dBm pulse. As the pulse width became longer, the absorbing performance decreased, approaching the high-power CW performance in Figs. 2(e) and 2(f). (c) Simulation result at 4.2 GHz with a 15 dBm pulse without capacitors. The pulse width dependence disappeared by removing capacitors which play an important role in exhibiting waveform dependence.

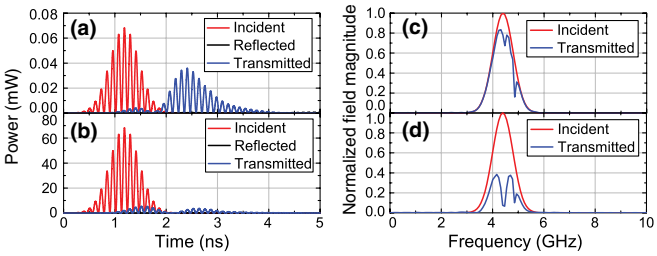

FIG. 4 (color online). Response to a Gaussian pulse modulated by a cosine function. (a) Low-power response and (b) high-power response. The frequency spectrum of each figure is seen in (c) and (d), respectively. In these figures the field magnitudes were normalized to the maxima of the incident electric fields. These figures also describe the bandwidth of the incident Gaussian pulse (see the red curves).

capacitors play an important role as shown in Fig. 3(c), where the same simulation as Fig. 3(a) was performed but without capacitors (see Supplemental Material [16] for more details such as low-power and high-power absorptance). Clearly, the pulse-width dependence seen in Fig. 3(a) disappeared here, since there was no capacitor to temporarily store the rectified energy. In other words, capacitors are indispensable for creating the waveform dependence, which, as explained above, can be controlled by the resistance and capacitance used.

Such flexible absorbing performance can be seen with a broadband Gaussian pulse. This type of short pulse can be assumed to be closer to realistic high-power threats to electronics from the viewpoint of the pulse width and frequency spectrum. The simulation results are shown in Fig. 4, where a Gaussian pulse was modulated by a cosine function so that the resultant frequency spectrum is the red curve of Fig. 4(c) (see Supplemental Material [16] for more details on the pulse). In Fig. 4(a), a low-power Gaussian pulse illuminated the metasurface, resulting in 70% energy transmission with 3% reflection, i.e., only 27 % absorption. The absorbing performance was markedly enhanced to 85%, when the input power was increased by a factor of 1,000 as in Fig. 4(b). Comparison between Figs. 4(c) and 4(d) reveals a significant reduction of the transmitted signal around 4.2 GHz, where our metasurface exhibited strong absorptance [see Fig. 2(c)].

The absorbing performance of our metasurface can be further enhanced by increasing the thickness of the substrate. Note that the thickness was only about $\lambda/50$ here, representing a very thin metasurface. However, the metasurface still exhibited dependence on the incoming power level as well as on the waveform. In addition, in order to simplify the simulation and measurement process, we tested the metasurface in waveguides. This indicates that use of a signal source that generates only a surface wave can more clearly show the difference. Furthermore, we used Schottky diodes in this study. However, the use of varactor diodes may enable us to sense the frequency of the incoming wave and tune the absorbing performance by varying the capacitance. We expect this would allow us to further improve the bandwidth of the nonlinear metasurface.

Use of rectification circuits can be seen in past studies [17,18], where diodes were used for antenna applications to rectify the incoming signal, resulting in, for example, extracting harmonics or behaving as an artificial magnetic conductor. However, for these purposes, it was not suitable to store the incoming energy temporarily and dissipate it, which is the key factor enabling the waveform dependence of the present structure.

Our metasurface absorber effectively dissipated most of the energy of high-power surface currents. This strong absorbing performance might appear similar to those of other metamaterial absorbers [19–23]. However, while these metamaterial absorbers focused on absorption of waves illuminated from free space, our metasurface is specifically designed for high-power surface currents. Nonetheless, our design is expected to respond to free space waves as well. The primary novelty of the nonlinear absorber described here is that it is the first surface designed specifically to respond to high-power pulsed signals, thus representing the first waveform-dependent absorber. Additionally, the demonstrated metasurface was 162 mm long, which is about two wavelengths at 4 GHz near the absorption peak. This indicates that applying the nonlinear metasurface around only a two-wavelength radius from sensitive electronics may be enough to protect them from high-power threats while still allowing them to communicate with external signal sources.

We have introduced a new kind of nonlinear metasurface that is designed for absorption for high-power microwave pulses. This surface works by rectifying the incoming signal using diodes, and storing the static field in capacitors, to be dissipated in resistors between pulses. Thus, the surface responds not only to the power level but also to the temporal profile of the incoming signal in order to specifically absorb short, high-power microwave pulses.

This work was supported by the Office Naval Research under Grant No. N00014–11–1–0460.

*Present address: Nagoya Institute of Technology, Gokiso-cho, Showa-ku, Nagoya, Aichi 466-8555, Japan.
hirokiwaka@gmail.com
†dsievenpiper@eng.ucsd.edu

[1] E. Knott, *Radar Cross Section Measurements* (SciTech Publishing, Raleigh, NC, 2006).
[2] B. A. Munk, *Frequency Selective Surfaces: Theory and Design* (Wiley, New York, 2000).
[3] A. A. Zharov, I. V. Shadrivov, and Y. S. Kivshar, Phys. Rev. Lett. **91**, 037401 (2003).
[4] H.-T. Chen, J. F. O'Hara, A. K. Azad, A. J. Taylor, R. D. Averitt, D. B. Shrekenhamer, and W. J. Padilla, Nat. Photonics **2**, 295 (2008).

[5] H. Chen, W. J. Padilla, J. M. O. Zide, A. C. Gossard, A. J. Taylor, and R. D. Averitt, Nature (London) **444**, 597 (2006).
[6] T. Driscoll, H. Kim, B. Chae, B. Kim, Y. Lee, N. Jokerst, S. Palit, D. Smith, M. Di Ventra, and D. Basov, Science **325**, 1518 (2009).
[7] M. Liu, H. Y. Hwang, H. Tao, A. C. Strikwerda, K. Fan, G. R. Keiser, A. J. Sternbach, K. G. West, S. Kittiwatanakul, J. Lu *et al.*, Nature (London) **487**, 345 (2012).
[8] H. Tao, A. C. Strikwerda, K. Fan, W. J. Padilla, X. Zhang, and R. D. Averitt, Phys. Rev. Lett. **103**, 147401 (2009).
[9] M. Lapine, I. V. Shadrivov, D. A. Powell, and Y. S. Kivshar, Sci. Rep. **1**, 138 (2011).
[10] M. Lapine, I. V. Shadrivov, D. A. Powell, and Y. S. Kivshar, Nat. Mater. **11**, 30 (2011).
[11] M. Klein, C. Enkrich, M. Wegener, and S. Linden, Science **313**, 502 (2006).
[12] Z. Wang, Y. Luo, L. Peng, J. Huangfu, T. Jiang, D. Wang, H. Chen, and L. Ran, Appl. Phys. Lett. **94**, 134102 (2009).
[13] E. Kim, F. Wang, W. Wu, Z. Yu, and Y. R. Shen, Phys. Rev. B **78**, 113102 (2008).
[14] H. Wakatsuchi, S. Kim, J. J. Rushton, and D. F. Sievenpiper, Appl. Phys. Lett. **102**, 214103 (2013).
[15] D. Sievenpiper, IEEE Antennas Wireless Propag. Lett. **10**, 1516 (2011).
[16] See Supplemental Material at http://link.aps.org/supplemental/10.1103/PhysRevLett.111.245501 for descriptions of the materials and methods of both simulations and measurements.
[17] F. Auzanneau and R. W. Ziolkowski, IEEE Trans. Microwave Theory Tech. **46**, 1628 (1998).
[18] F. Auzanneau and R. W. Ziolkowski, IEEE Trans. Antennas Propag. **47**, 1330 (1999).
[19] N. I. Landy, S. Sajuyigbe, J. J. Mock, D. R. Smith, and W. J. Padilla, Phys. Rev. Lett. **100**, 207402 (2008).
[20] D. J. Kern and D. H. Werner, Microw. Opt. Technol. Lett. **38**, 61 (2003).
[21] H. Wakatsuchi, S. Greedy, C. Christopoulos, and J. Paul, Opt. Express **18**, 22187 (2010).
[22] H. Wakatsuchi and C. Christopoulos, Appl. Phys. Lett. **98**, 221105 (2011).
[23] H. Wakatsuchi, J. Paul, and C. Christopoulos, IEEE Trans. Antennas Propag. **60**, 5743 (2012).